Advanced Steel Construction – Vol. 20 No. 1 (2024) 30–38
DOI:10.18057/IJASC.2024.20.1.4

EVALUATION OF LOCAL-PLATE BUCKLING COEFFICIENT FOR THE DESIGN OF COLD-FORMED STEEL-LIPPED CHANNEL CROSS SECTIONS: NUMERICAL SIMULATIONS AND DESIGN RECOMMENDATIONS

Hadeer Mashaly [1], A.H.A Abdelrahman [2,*], Fikry A. Salem [2] and Nabil S. Mahmoud [2]

[1] *Civil Engineering Department, Faculty of Engineering, Horus University, New Damietta, Egypt*
[2] *Structural Engineering Department, Faculty of Engineering, Mansoura University, Mansoura, Egypt*
** (Corresponding author: E-mail: a_hussain@mans.edu.eg)*

ABSTRACT

Recent advancements in design guidelines for cold-formed steel members focus on enhancing the prediction of nominal strengths under various loading conditions. This improvement is achieved through precise accounting for local plate buckling behavior. Nevertheless, the Effective-Width Method (EWM), aligned with current design standards, estimates a lower structural capacity for cold-formed steel members. Assuming buckling precedes the yielding of cross-sections and considering no interactive restraint between adjacent elements, conservative predictions of member strengths are derived. To address this issue, this paper introduces a numerical investigation involving several lipped channel cross-sections with varying web height-to-flange width ratios, intending to assess the local plate buckling coefficient (k-value). Initially, validating a shell finite-element model against test results establishes benchmark strengths for the considered cross-sections. Subsequently, analytical solutions for calculating the k-value are presented and compared with those obtained from numerical solutions. Interactions between cross-sectional adjacent elements are examined, leading to a proposed refined EWM compliant with AISI standards. Finally, a reliability analysis is performed to illustrate the accuracy and reliability of the proposed design method. This research highlights the significance of accurately considering the restraining effect between sectional sub-elements and the importance of boundary conditions influencing the plate buckling coefficient.

ARTICLE HISTORY

Received: 13 October 2023
Revised: 13 October 2023
Accepted: 18 November 2023

KEYWORDS

Local buckling;
Finite element;
Lipped channel;
Buckling coefficient;
Analytical expressions

1. Introduction

Modern structural technology prioritizes environmental practices to mitigate global energy depletion, whether in construction, operation, maintenance, or demolition. Cold-formed steel (CFS) emerges as an eco-friendly and recyclable structural material, minimizing carbon dioxide emissions during its cold-forming process, unlike hot-rolled steel sections that demand higher thermal energy. As a primary load-bearing material, CFS optimizes construction purposes due to its numerous advantages, including a high strength-to-weight ratio, easy installation, and lower energy consumption. It finds wide-ranging applications in construction manufacturing, such as light and short-span structures, light partition walls, and storage rack structures. CFS, derived from the flexion of thin-walled steel sheets, is susceptible to various buckling phenomena, including local buckling (L), distortional buckling (D), and global buckling (G) as. These instability modes exhibit elastic buckling loads before reaching ultimate strength and exhibiting post-buckling behavior. Consequently, the hot-rolled steel design approach is unsuitable for CFS, necessitating advanced guidance in three key areas: i) experimental tests to explore various CFS cross-sections under different load conditions [1]–[10], ii) numerical analyses, such as the finite strip method [11], [12] and shell finite element models [13], offering accurate simulations with realistic geometric imperfections and residual stresses, and iii) the development of simplified design standards [14]–[17] to provide accessible and semi-accurate guidance for the design of CFS sections, reducing reliance on more complex and expensive tools.

Two existing design theories play a pivotal role in assessing the structural capacity of CFS axial columns and flexural beams: the traditional Effective Width Method (EWM) and the recently advanced Direct Strength Method (DSM). The former employs iterative solutions to define the effective width for each element comprising the cross-section. In contrast, the DSM calculates elastic buckling loads in local, distortional, and global buckling modes, addressing cross-section instability and predicting the nominal strength for each buckling mode. Consequently, numerous researchers have dedicated their efforts to examining the buckling behavior of CFS lipped-channel sections under diverse loading and boundary conditions. For example, Bryan [18] derived a solution for critical local buckling stress and the plate buckling coefficient for simply supported plates subjected to compression. Subsequent studies explored different boundary and loading conditions, revealing that the nominal plate strength is independent of critical elastic buckling theory, as noted in [19], due to post-buckling behavior. Kármán [20] delved into nominal buckling strength based on elastic buckling solutions, introducing empirical factors for simply supported plates. Winter [7], in later work, adapted the elastic buckling solution, presenting a formula for nominal plate strength during post-buckling behavior. This formula remains integral to current effective width approaches, including AISI [15] and Eurocode3 (EC3) [16], and is incorporated into various contemporary design methodologies.

More recently, a design theory based on DSM has emerged [14], [21], relying on determining the critical elastic buckling stress for entire cross-sections. Currently, this method is employed in Australia/New Zealand and North America standards.

Taking inspiration from prior investigations, the EWM treated the plate element as simply supported, overlooking any interaction or restraining strength with adjacent elements. Consequently, the predicted nominal post-buckling strength proves conservative when compared to experimental test results. Yu and Yan [22] illustrated the influence of the web height-to-flange width (H/B) ratio on the plate buckling coefficient in the C and Z sections. Mulligan and Pekoz [23] conducted experiments on lipped channel stub columns to quantify local buckling and inspected buckling coefficient values for cross-section sub-elements (web, flange, and stiffener). These values, derived from experimental results, were lower than those for simply supported plate elements due to the consideration of interaction between adjacent elements. Consequently, the impact of the H/B ratio on nominal strength, attributed to the interaction effect, is emphasized. An increase in cross-section width provides support to the web element, thereby increasing nominal buckling strength. This interaction significantly influences the buckling coefficient value (k), primarily dependent on boundary conditions and stress gradient.

This research contributes to advancing the effective width method (EWM) by incorporating elastic local buckling phenomena in assessing the plate buckling coefficient (k), a parameter significantly influenced by the interaction between adjacent sub-elements. Initially, literature-derived test results are employed to validate a newly developed 2D shell finite-element model (SFEM) using ABAQUS [13]. The SFEM incorporates appropriate geometric imperfections and material properties specific to CFS. Subsequently, finite strip analysis in CUFSM [11] is utilized to perform elastic local buckling solutions, which are then compared with various expressions for local plate buckling coefficients in the calculation of critical local buckling stress (F_{cr}). This comparison characterizes the restraining effect between adjacent sub-elements and demonstrates superior performance in representing elastic behavior. The illustration of various elements and analytical methods with different buckling coefficients within the EWM theory is also outlined. These methods are presented to evaluate the impact of restraining interaction between connected sub-elements with varying boundary conditions. Results obtained from the

Direct Strength Method (DSM) are also discussed, revealing that enhancing elastic stability for the gross cross-section may be more accurate than the EWM. Subsequently, after presenting diverse design approaches for CFS, a parametric study is conducted on different CFS-lipped channel cross-sections with various web height-to-flange width ratios. These results are then compared to outcomes from the developed and validated shell finite element models (SFEM) [25-26], which serve as benchmark results for evaluating the reliability of the proposed refined design method (i.e., AISI-Re). This refined method aims to obtain optimum nominal strength for CFS-lipped channel cross-sections. Finally, the findings are summarized, emphasizing the role of the plate buckling coefficient (k) in determining the nominal buckling strength.

2. Finite element modelling

2.1. Shell finite element modeling

Finite Element (FE) analysis is used in ABAQUS [13] to analyze the behavior of thin plates, simulating the experimental tests detailed in [25] and [26]. The linear 4-node shell element with reduced integration (S4R) is selected for modeling the CFS columns. As mentioned in [27], this shell element aligns with the study's goals, which focus on local plate buckling. Based on mesh sensitivity analysis, a maximum mesh size of 5 mm x 5 mm is assumed in element discretization, guaranteeing precise and trustworthy results for a comprehensive parametric investigation. Four elements are used to model the rounded corners of the lipped channel cross-section.

2.2. Modelling parameters

The benchmark experimental settings for the specimens under test were included in the simulations. A 600S137-54 lipped-channel cross-section with an intermediate length of 610 mm was one of the geometrical attributes that were subjected to several loading combinations (axial, uniaxial, and biaxial eccentricities). The reference point was established using a kinematic coupling constraint connecting it to the end cross-sections, and it was situated at the cross-section centroid. With pin-ended boundary conditions, every beam-column was simulated. According to [25], Young's modulus was 203.4 GPa, and the steel yield stress was 364.5 MPa. To construct the real stress-strain curve and account for the inelastic behavior of CFS due to material nonlinearity, the two-stage Ramberg-Osgood model, as presented by Gardner and Yun [31], was used. Initial geometric imperfections were incorporated to thoroughly evaluate the simulations against the experimental tests. This allowed for proper parametric investigations of CFS behavior and demonstrated satisfactory agreement with the results. To ensure the accuracy of the finite element modeling, additional test specimens from various experimental tests were simulated under the same standard conditions to account for pure compression and local buckling failure modes, as detailed in [25].

2.3. Residual stresses and cold-forming effect

The same manufacturing process, including coiling, uncoiling, and shape bending, causes residual stresses and cold-forming effects. Residual stresses show a drop in yield strength, but the cold-forming process raises the yield strength in the corner region, leading to greater strength. The most accurate way to estimate a member's true strength is to model the manufacturing process, including cold-forming effects and residual stresses. While this is frequently a difficult process to carry out, it is essential to avoid modeling them individually. According to several studies, there is no noticeable correlation between residual stress and the final capacity of columns (e.g., Schafer and Peköz; Abdel-Rahman and Sivakumaran; Ellobody and Young) [28-30]. As long as ultimate load capacity is the main consideration, the yield strength in the corner region is enhanced due to the cold-forming process, which reduces the effect of residual stress. The corner effect and residual stress, especially in post-ultimate behavior, significantly affect column behavior but do not affect the final load capacity value, according to Abdel-Rahman and Sivakumaran [29]. This study disregarded the residual stress and corner enhancement in the FE model since it focuses on the ultimate load capacity rather than the post-ultimate load behavior.

2.4. Initial geometrical imperfections

Initial geometric imperfections are introduced by executing the linear perturbation "Buckle" step, enabling the prediction of the buckling mode shape to be scaled within the subsequent nonlinear collapse analysis. Drawing from prior research, various imperfection amplitudes are integrated into the model to ensure thorough validation and accurate verification. The specific amplitude values are outlined in Table 1, along with their corresponding peak loads.

The FE results show that when the imperfection amplitude is adjusted to $6te^{-2t}$, as suggested by Schafer and Peköz [32], the predicted peak loads show good agreement with the experimental test results. Values produced by this configuration are most similar to the experimental findings; mean predicted-to-test ratios for [25] and [26] are 1.0047 and 1.1091, respectively. The coefficients of variation (COV) that correspond to these values are 0.0337 and 0.1287, respectively. For this reason, to make the solutions in the current study seem more realistic, this specific amplitude value was chosen.

Table 1
Peak ultimate loads for experimental and FE results with different imperfection amplitudes

	Specimen	Imperfection magnitude					
		0.24mm	0.005t	t/10	d/400	Schafer and Peköz [32]	Dawson and Walker [33]
Torabian et al, [25]	600S137-54 (1)	0.9964	1.0165	0.9966	0.9945	0.9933	0.9949
	600S137-54 (2)	0.9868	1.0408	0.9883	0.9841	0.9827	1.0405
	600S137-54 (3)	0.9743	1.0855	0.9754	0.9730	0.9700	1.0715
	600S137-54 (4)	1.0264	1.0325	1.0279	1.0250	1.0236	1.0308
	600S137-54 (5)	1.0733	1.1110	1.0897	1.0616	1.0538	1.1126
	Mean	**1.0114**	**1.0573**	**1.0156**	**1.0076**	**1.0047**	**1.0501**
	COV	**0.0391**	**0.0373**	**0.0450**	**0.0356**	**0.0337**	**0.0423**
Roy et al, [26]	C75-L500-1	1.1089	1.1292	1.1202	1.1154	1.0789	1.2345
	C75-L500-2	1.3387	0.0000	1.3732	1.3661	1.2951	1.5421
	C75-L500-3	1.2008	1.2716	1.2090	1.2152	1.2060	1.5023
	C90-L500-1	0.9594	0.9650	0.9676	0.9643	0.9346	1.0416
	C90-L500-2	1.0641	1.1819	1.0910	1.0853	1.0310	1.0074
	Mean	**1.1344**	**0.9095**	**1.1522**	**1.1493**	**1.1091**	**1.2656**
	COV	**0.1265**	**0.5723**	**0.1309**	**0.1311**	**0.1287**	**0.1976**

2.5. Validation and verifications

A noteworthy agreement between FE results and test results in terms of load-displacement response, peak loads (Fig. 1), and failure modes (Fig. 2) is illustrated visually by the results of FE modeling and experimental tests [25]. Furthermore, the ultimate loads from the experiments and FE models are compiled in Table 2. A comparatively low coefficient of variation (COV) of 0.06 accompanies the mean test-to-predicted value of 0.98. Overall, the findings shown in Figs. (1-2) and Table 2 demonstrate that the developed FE models can reliably and efficiently simulate the behavior of lipped-channel sections made of CFS under various loading conditions and buckling modes.

Table 2
Comparisons between test and FE results [25-26]

Specimen	Test		FE		Comparison P_{test}/P_{FE}
	P_{test} (KN)	Buckling Mode	P_{FE} (KN)	Buckling Mode	
600S137-54 (No. 1)	18.09	L	17.9683	L	1.0068
600S137-54 (No. 2)	28.25	L	27.7602	L	1.0176
600S137-54 (No. 3)	43.38	L	42.0804	L	1.0309
600S137-54 (No. 4)	46.86	D	47.9669	D	0.9769
600S137-54 (No. 5)	24.99	D	26.3336	D	0.9490
C75-L500-1	42.20	L	43.004	L	0.9813
C75-L500-2	50.10	L	59.4223	L	0.8431
C75-L500-3	75.90	L	80.187	L	0.9465
C90-L500-1	49.00	L	47.0097	L	1.0423
C90-L500-2	61.10	L	59.5379	L	1.0262
Mean					**0.9821**
COV					**0.0603**

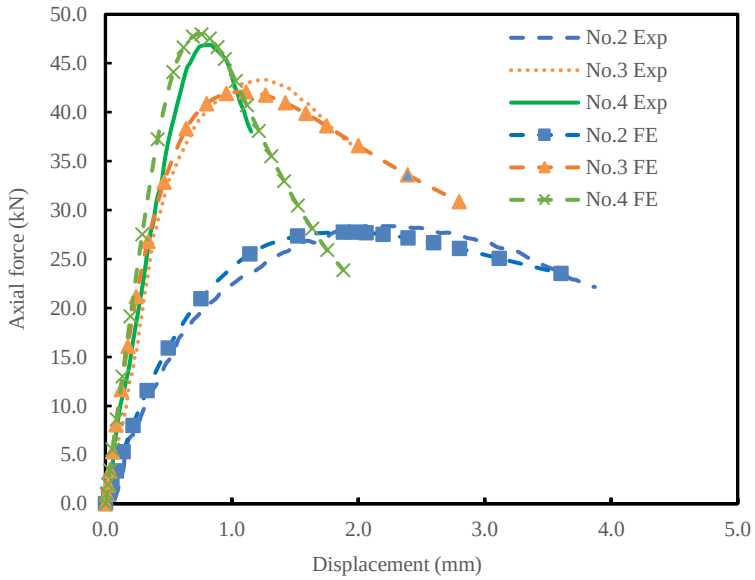

Fig. 1 Load-displacement curves from FEM and experimental tests by Torabian et al, [25]

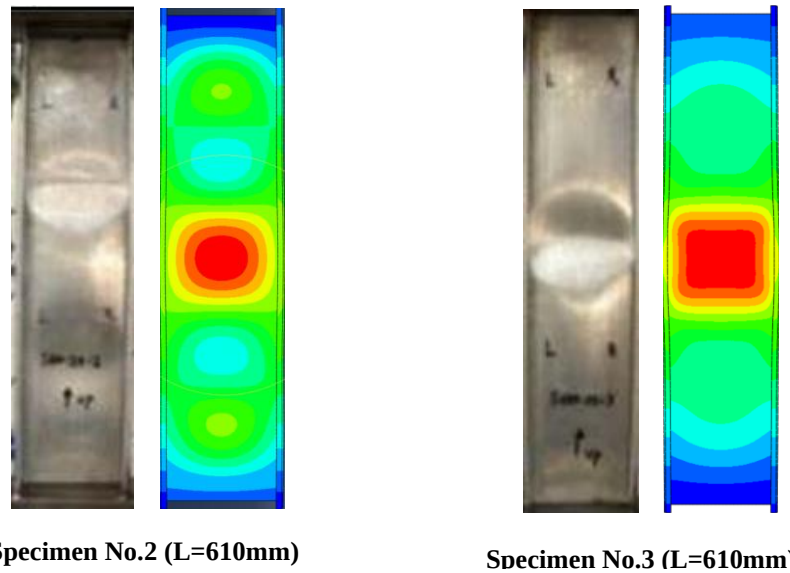

Fig. 2 Failure modes of experimental specimens from Torabian et al, [25] and FEM

3. Analytical solutions of local plate buckling coefficients

The critical local buckling stress (F_{crl}) is considered an essential and effective parameter in cold-formed steel design approaches such as the Direct Strength method (DSM) and Effective Width Method (EWM), whether in AISI [15] or EC3 [16], to compute the cross-sectional nominal strength. The general equation for the plate's critical local buckling stress is as follows:

$$F_{crl} = k_x \frac{\pi^2 E}{12(1-\nu^2)} \left(\frac{t}{x}\right)^2 \quad (1)$$

where k_x is the plate buckling coefficient, E is the modulus of elasticity, t is the plate thickness, ν is the Poisson's ratio of steel, and x is the plate width. Eq. (1) clarifies that the plate buckling coefficient (k_x) affects remarkably the critical local buckling stress (F_{crl}), which in turn affects the nominal strength of the cross-section. As a result, this study clarifies the various design standards and suggested formulas for determining the plate buckling coefficient and how it affects the ultimate strength prediction.

The critical local buckling stress for the lipped channel cross-section is found by taking the minimum local buckling stress of each element that makes up the cross-section. In the present investigation, and as per Eq. (1), four methods are employed to estimate the local buckling stress: 1) the element method, as incorporated in AISI S100 [15], 2) the approximate upper bounds for the element method (an analytical method detailed in [24]), 3) the current AISI [15], and 4) empirical closed-form equations proposed by Ahdab et al. [24].

3.1. The element method

The element method considers no interaction between adjacent elements, following AISI S100 [17]. As seen in Fig. 3, the elements are believed to be free at the unattached edge and simply supported at the attached edge. The plate buckling coefficient under pure compression or stress gradient is generally expressed in Eq. (2).

$$\boldsymbol{k_\psi = 4 + 2(1 - \psi^3) + (1 - \psi)} \quad (2)$$

where k_ψ is the plate buckling coefficient, $\psi = |F_2/F_1|$ is the determinant for the end plate stress ratio, and F_1 is the larger compressive stress at the end plate.

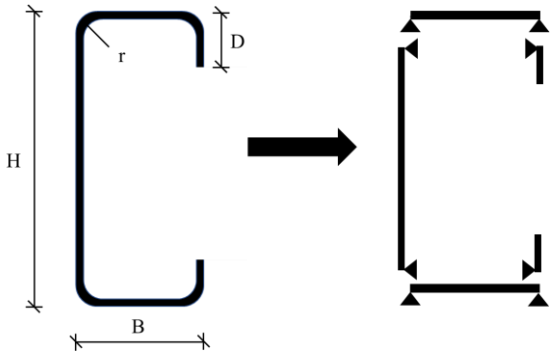

Fig. 3 Simply supported sub-elements in a lipped channel cross section based on the element method

3.2. Approximate upper bounds for element method (analytical method)

This approach assumes that every sub-element in the cross-section has a fixed end condition (Fig. 4), ignoring interactions with other elements. For local buckling solutions, it is acknowledged as a nonconservative method. To compute the plate buckling coefficient in line with the approximate upper bounds for the element method, Eq. (3) expands Eq. (2), which was first presented in [24].

$$\boldsymbol{k_\psi = 6.97 + 3.3(1 - \psi^3) + 3.3(1 - \psi)} \quad (3)$$

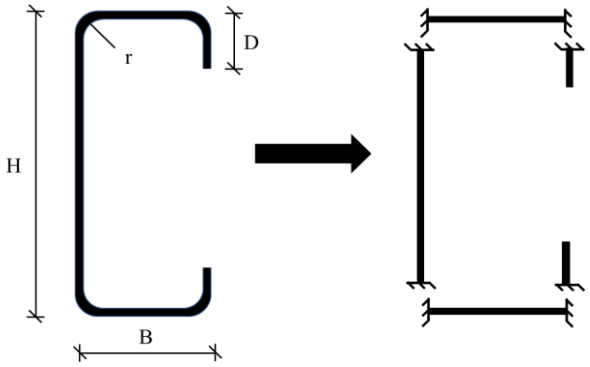

Fig. 4 Fixed supported sub-elements in lipped channel cross section based on the approximate upper bound method

3.3. The empirical closed-formed equation

Ahdab et al. [24] explored a different, semi-accurate method of calculating the plate buckling coefficient by using empirical closed-form equations that accounted for different loading conditions and took sub-element interaction into account. This method considers the geometry of adjacent elements within and beyond a diverse range of lipped channel cross-sections. The closed-form equation for pure compression is presented in Eq. (4), while those for major axis bending are given in Eqs. (5) and (6), as follows:

For $0 \le H/B \le 12$ and $0 \le D/B \le 1$

$$k_H = min\left(4.5\left(\frac{H}{B}\right)^2, 4\left[0.73\left(\frac{D}{B}\right)^{0.36} + 1\right]\right) \quad (4)$$

For $0 \le H/B \le 1$ and $0.15 \le D/B \le 0.4$

$$k_B = \max\left(0.3\left(\frac{B}{H}\right) + 5.2, 0.4\left(\frac{H}{B}\right) + 5.9\right) \ge k_{EWM\ AISI} \quad (5)$$

For $0 \le H/B \le 1$ and $0.15 \le D/B \le 0.4$

$$k_B = min\left(-0.4\left(\frac{H}{B}\right) + 5.9, 22.3\left(\frac{H}{B}\right)^{-1.8}\right) \ge k_{EWM\ AISI} \quad (6)$$

These closed-form equations are first compared with finite strip analysis (CUFSM) results for solutions involving elastic buckling. Subsequently, these are implemented in the AISI [15] methodology (henceforth referred to as AISI-Re) by substituting the current buckling coefficient values, thereby revealing their pivotal role in predicting the nominal buckling strength.

3.4. Results by finite strip method

The elastic buckling stress ($\boldsymbol{F_{cr}}$) for a range of cross-sections with varying web height-to-flange width ratios (H/B) was calculated by finite strip analysis using CUFSM [11]. B = 50.8 mm, D = 5.08 mm, t = 1.4376 mm, and r = 2.8752 mm are the cross-sectional dimensions. There is a 203.5 GPa Young's modulus (E) and a 0.3 Poisson's ratio (ν). Then, utilizing Eq. (1), the critical local buckling stresses were transformed into plate buckling coefficients $\boldsymbol{K_H}$, $\boldsymbol{K_B}$, and $\boldsymbol{K_D}$ so that the results could be compared to those obtained from Ahdab et al.'s closed-form equations [24]. In FSM within CUFSM, to prevent non-unique minima and allow for the automated study of elastic buckling modes in CFS members, the methodology for CUFSM utilization as described in [34] has been implemented. Accordingly, results are shown in Fig. 5 and comprise pure compression and major axis bending. Remarkably, there is a good agreement that validates the accuracy of elastic buckling stress prediction for lipped channel cross-sections. Fig. 5(a) shows that the web plate buckling coefficient under pure compression is slightly affected when the web-to-flange width ratio (H/B) is increased beyond two (≥ 2). On the other hand, as depicted in Fig. 5(b), the flange local buckling coefficient ($\boldsymbol{K_B}$) is significantly impacted by the elastic critical buckling stress ($\boldsymbol{F_{cr}}$) for major axis bending.

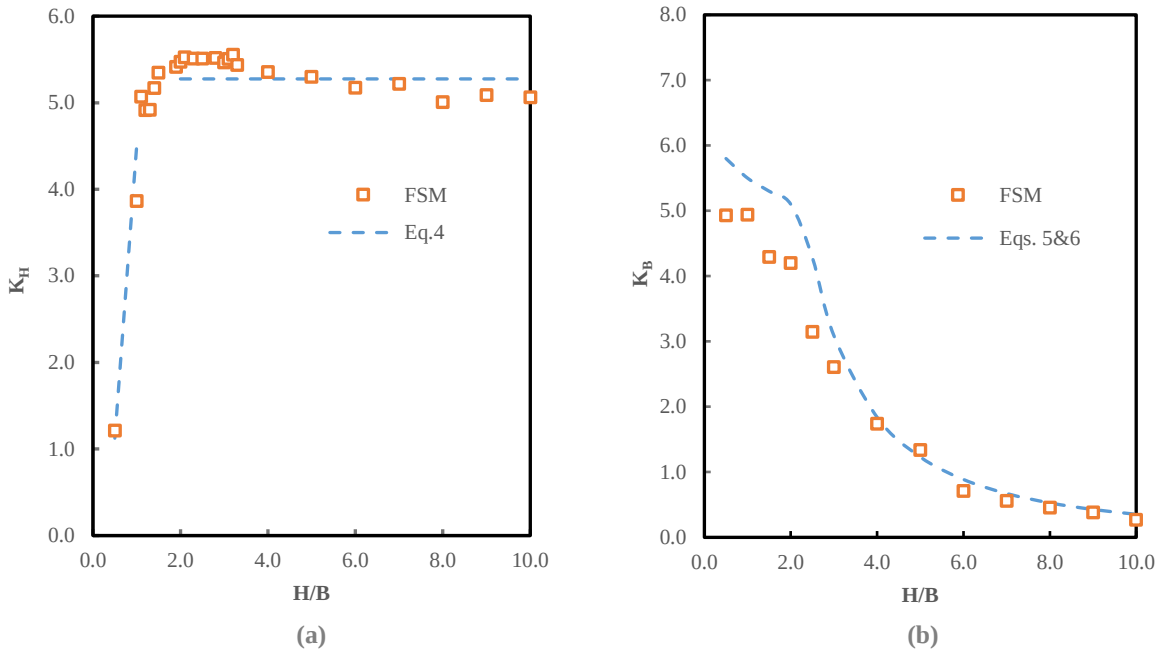

Fig. 5 Plate buckling coefficient versus H/B ratio (a) web buckling coefficients for pure compression, and (b) flange buckling coefficients for major axis bending

4. Design guidelines

4.1. Effective width method

The effective width method (EWM) is used by the current design standards, EC3 [16] and AISI [15], to estimate the nominal strength of columns and beam-columns. The EWM determines the effective width properties for each sub-element in the cross-section under uniform stress, thereby reducing the load-carrying capacity of a simply supported member. The effective width is determined by using Winter's Equation [7], which is given as follows;

$$b_{eff} = \frac{\left(1-\frac{0.22}{\lambda_p}\right)b}{\lambda_p} \leq b \tag{7}$$

$$\lambda_p = \sqrt{\left(\frac{F_y}{F_{crl}}\right)} \tag{8}$$

where b_{eff} is the effective width of the sub-element, λ_p is the slenderness parameter, b is the gross width, F_y is the yield stress, and F_{crl} is the critical local buckling stress of the sub-element, which is calculated from Eq.(1). The modern CFS design specifications make extensive use of the effective width method (EWM). This method relies on figuring out each sub-element's plate buckling coefficient (k), which is important to determine the critical local buckling stress (F_{crl}) and, in turn, the effective width properties. The plate buckling coefficient (k) for stiffened, and unstiffened elements mainly depends on the stress distribution inside the element and the current boundary conditions. For example, AISI considers the effect of the nearby stiffener in lipped channels when calculating the plate buckling coefficient of the compression flange. It is important to note that EWM tends to conservatively estimate the ultimate buckling strength of the considered CFS cross-sections under diverse loading conditions [25]. The adopted values of the local plate buckling coefficients (k), which do not consider the interactions between adjacent sub-elements, are responsible for this conservatism in the effective width properties.

4.2. Direct strength method

The direct strength method (DSM) has recently emerged as an alternative approach, explicitly outlined in Appendix 1 of the AISI specification [21]. This method determines nominal strength through finite strip analysis, finite element analysis, or closed-form solutions, accounting for elastic buckling loads and interactions between sub-elements. Through elastic buckling analysis, the DSM optimizes the use of gross cross-sectional properties. It identifies the three elastic buckling modes (L, D, and G) over the whole cross-section and determines which mode controls the nominal strength. According to previous studies, for lipped channel cross-sections, the DSM's findings are often slightly higher than the EWM's [25]. A summary of the DSM design equations under pure compression is provided as follows:
For global buckling, the nominal strength P_{ne} is calculated from

$$P_{ne} = \left(0.658^{\lambda_c^2}\right) A * F_y \quad For\ \lambda_c \leq 1.5 \tag{9}$$

$$P_{ne} = \left(\frac{0.877}{(\lambda_c^2)}\right) A * F_y \quad For\ \lambda_c > 1.5 \tag{10}$$

$$\lambda_c = \sqrt{\frac{P_y}{P_{cre}}} \tag{11}$$

$$P_{nl} = P_{ne} \quad For\ \lambda_c \leq 0.776 \tag{12}$$

$$P_{nl} = \left[1 - 0.15 * \left(\frac{P_{crl}}{P_{ne}}\right)^{0.4}\right]\left(\frac{P_{crl}}{P_{ne}}\right)^{0.4} P_{ne} \quad For\ \lambda_c > 0.776 \tag{13}$$

$$P_{crl} = A * F_{cr} \tag{14}$$

Nominal Strength for beam column M_{nl} is calculated from equations of the same trend detailed in [21].

5. Refined AISI method (AISI-Re)

In this section, the empirical closed-form equations for the plate buckling coefficient (k) are applied within AISI to predict the nominal ultimate strength, referred to as AISI-Re, intending to achieve two objectives: 1) evaluate the proposed value of the local plate buckling coefficient in light of the current AISI specifications; and 2) conduct a comprehensive parametric study on the nominal strength of various lipped channel columns and beam-columns, quantifying the impact of the buckling coefficient (k) on the predicted strength. Finally, a reliability analysis will more accurately show how the suggested method (AISI-Re) has improved validity compared to the present AISI recommendations.

5.1. Parametric study

A comprehensive parametric study was undertaken on various lipped channel cross-sections under compression and major axis bending. The study focused on local buckling failure modes, employing models of relatively short member lengths (L) by adopting L=H to present an analytical exploration of the

elastic buckling and post-buckling behavior of lipped channel cross-sections. The EWM was utilized, incorporating four k-values for local plate buckling: 1) following AISI specifications, 2) AISI with k-value by element method (AISI-Elem), 3) AISI with k-value by analytical method (AISI-Ana), and 4) AISI-Re with k-value by Ahdab et al., [24], considering interactions between adjacent sub-elements. The only difference between these approaches is the value that is determined for the plate buckling coefficient (i.e., k value), which in turn affects the nominal strength for the typical cross-section. The Young's modulus, the material yield stress, and Poisson's ratio are taken as E = 210 GPa, F_y = 345 MPa, and $\nu = 0.3$, respectively. Results based on EWM with different k values are compared with those obtained from SFEM that represent validated simulations for experimental tests. The dimension parameters include web height (H = 70 mm), thickness (t = 1.5 mm), inner corner radius (R = 2 mm), stiffener length over flange width ratio (D/B = 0.2) to avoid large lip stiffeners and eliminate their effect on the element's theoretical buckling stress [35], and the (H/B) ratio varies with a range from 1 to 2.

5.1.1. Axial compression

As per several design approaches and finite element (FE) models, Fig. 6 shows the web height to flange width ratio (H/B) effect on the nominal strength of different cross-sections under pure compression. All existing design methods and solutions show significant conservatism, with the FE models providing the maximum nominal strength. Since AISI-Ana corresponds to an upper-bound philosophy, it produces the higher results. These curves demonstrate that the direct strength method (DSM) is a less conservative method than AISI for the cross-sections under study. On the other hand, the results from AISI-Re are more compatible with FE models and perform effectively when compared to the present AISI specifications. This can be attributed to implementing more accurate and reliable equations for calculating the plate buckling coefficient (k). Furthermore, it is observed that the nominal strength increases with an increasing H/B ratio up to a specified level when it remains relatively constant. Similar trends are noticed across different design methods. An increase in the H/B ratio up to 1.8 is shown to have a slight effect on the P_n/P_y ratio. With regard to the absence of the flange's local buckling and an increase in the web's local buckling, decreasing the flange width (B) lowers the nominal strength. AISI and AISI-Elem provide almost identical results for (H/B) higher than 1.75, as the flange-lip interaction gradually disappears in AISI when the flange width (B) is decreased. In summary, the sectional dimensions and predicted-to-FE results based on AISI and AISI-Re are presented in Table 3. The mean $P_{predicted}/P_{FE}$ ratio is 0.89 and 0.83, respectively, with corresponding COV values of 0.01 and 0.05. This reconfirms and demonstrates the higher accuracy and reliability of the proposed AISI-Re compared to the current AISI design guidelines.

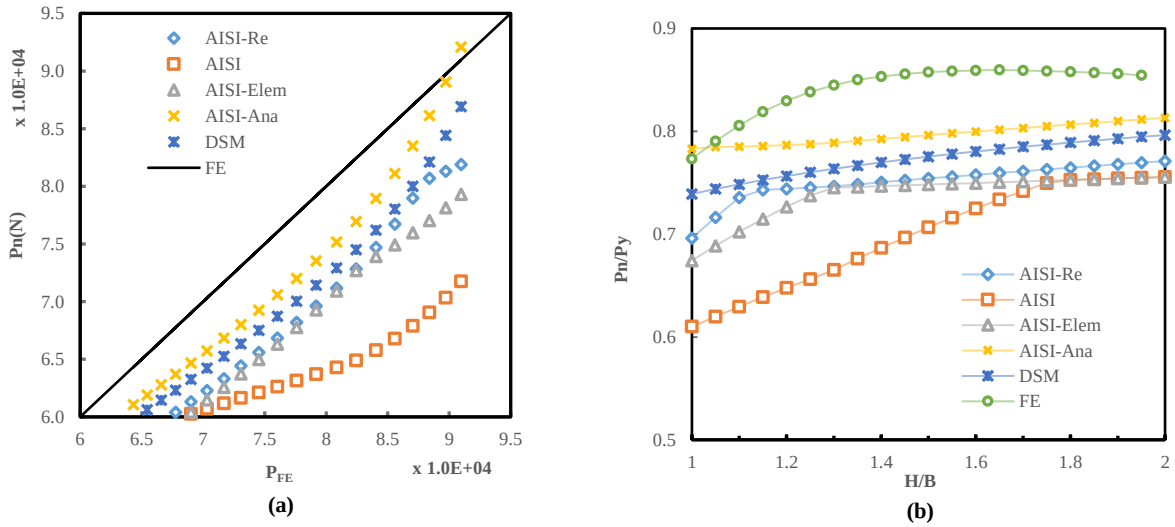

Fig. 6 Comparisons between nominal axial strengths from different design methods and FE results: (a) $\mathbf{P_{FE}}$ versus $\mathbf{P_{predicted}}$, and (b) normalized predicted loads versus H/B ratio

Table 2
Section properties and comparisons between FE results and different design standards for lipped channels under pure compression

No.	H (mm)	H/B	B (mm)	C (mm)	T (mm)	R (mm)	$P_{AISI-Re}/P_{FE}$	P_{AISI}/P_{FE}
1	70	1	70.00	14.00	1.5	2	0.90	0.79
2	70	1.05	66.67	13.33	1.5	2	0.91	0.78
3	70	1.1	63.64	12.73	1.5	2	0.91	0.78
4	70	1.15	60.87	12.17	1.5	2	0.91	0.78
5	70	1.2	58.33	11.67	1.5	2	0.90	0.78
6	70	1.25	56.00	11.20	1.5	2	0.89	0.78
7	70	1.3	53.85	10.77	1.5	2	0.88	0.79
8	70	1.35	51.85	10.37	1.5	2	0.88	0.80
9	70	1.4	50.00	10.00	1.5	2	0.88	0.80
10	70	1.45	48.28	9.66	1.5	2	0.88	0.81
11	70	1.5	46.67	9.33	1.5	2	0.88	0.82
12	70	1.55	45.16	9.03	1.5	2	0.88	0.83
13	70	1.6	43.75	8.75	1.5	2	0.88	0.84
14	70	1.65	42.42	8.48	1.5	2	0.88	0.85
15	70	1.7	41.18	8.24	1.5	2	0.89	0.86
16	70	1.75	40.00	8.00	1.5	2	0.89	0.87
17	70	1.8	38.89	7.78	1.5	2	0.89	0.88
18	70	1.85	37.84	7.57	1.5	2	0.89	0.88
19	70	1.9	36.84	7.37	1.5	2	0.90	0.88
20	70	1.95	35.90	7.18	1.5	2	0.90	0.88
						Mean	**0.89**	**0.83**
						COV	**0.01**	**0.05**

5.1.2. Eccentric compression

A similar parametric study is conducted on cross-sections exposed to major axis bending to improve the prediction of beam-column cross-section strength. The goal is to evaluate the accuracy of different flexural nominal strength prediction methods by comparing their results with benchmark SFEM data. As described in AISI [15], a simple linear interaction equation (Eq. (15)) is used to quantify the effect of varying eccentricities on nominal flexural strength for different cross-sections.

$$\frac{\bar{P}}{P_a} + \frac{\bar{M}_x}{M_{ax}} \leq 1.0 \qquad (15)$$

where

$\bar{P}$ = required compressive axial strength (obtained from FEM models)

P_a = nominal design strength obtained from different design approaches.

$\bar{M}_x$ =required flexural strengths ($= \bar{P} * eccentricity$)

M_{ax} = nominal flexural strengths according to different design approaches.

As shown in Fig. 7, nearly all of the results obtained using the different methods (AISI, AISI-Elem, AISI-Ana, and AISI-Re) are similar for (H/B) greater than 1.65, suggesting that the effective width (i.e., a reduction factor (ρ=1) for each sub-element) is fully used. Because of the reduced interaction between the web and flange and the minor amount of web local buckling seen under major axis bending, it can be concluded that reducing the flange width (B) does not affect the nominal strength of flexural beams. Alternatively, for larger (H/B) ratios, the direct strength method (DSM) produces more conservative results than the effective width method (EWM) because, as reported in [36], decreasing the flange width (B) reduces the elastic buckling stress for the whole gross section, which in turn lowers the nominal strength of the member. In contrast, EWM calculates the critical buckling stress for each element separately. Furthermore, major axis bending supports the web, with its half-height experiencing tension. The nominal strength value is substantially enhanced by AISI-Re under different eccentricities (e.g., e = H/10, H/5, H/2, or H), as shown in Fig. 8, with the fact that it exhibits less conservative M_n/M_y values than prior approaches. It is obvious that the EWM can significantly enhance the prediction of nominal strength by including k of AISI-Re. However, in this case, the EWM continuously underestimates the nominal strength of the analyzed beam columns, independent of the applied k-values. The simpler and more linear interaction equations [1] established for eccentrically loaded lipped channels cause this disparity. Finally, Table 4 presents the summary of predicted-to-FE results. The corresponding mean and COV values confirm the reliability of the suggested AISI-Re method.

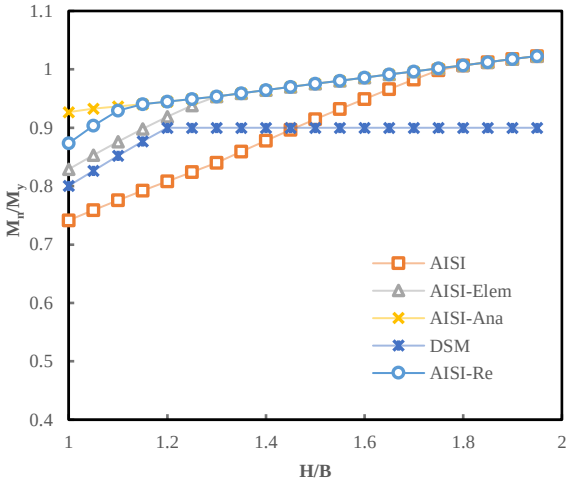

Fig. 7 Comparisons between different design methods and FE results for flexural beams

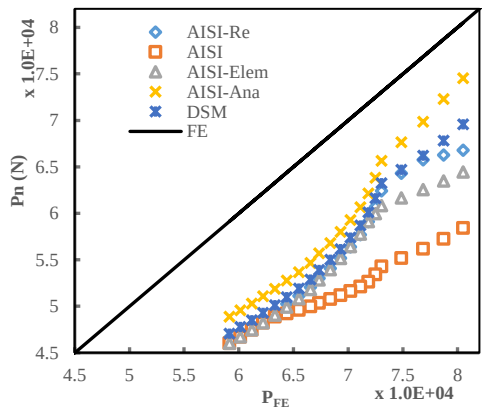

(a) e=H/10

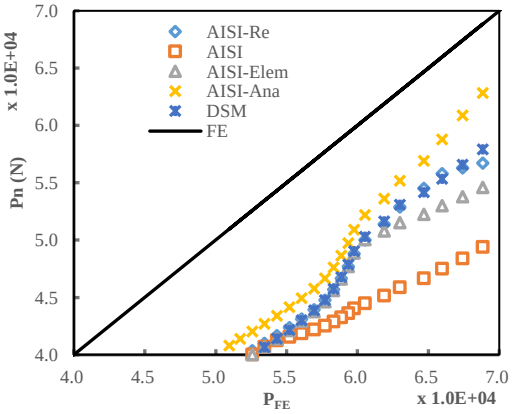

(b) e=H/5

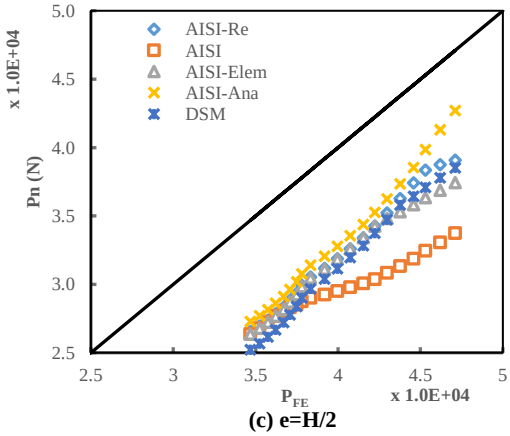

(c) e=H/2

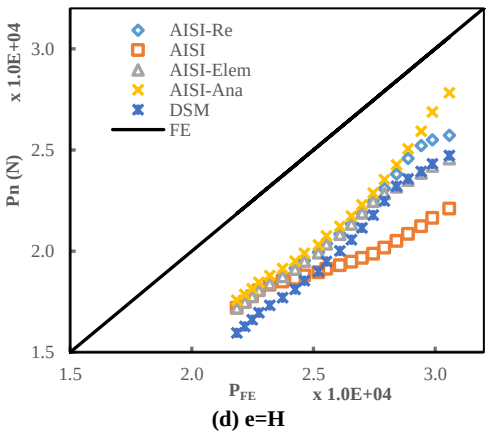

(d) e=H

Fig. 8 Comparisons between different design methods and FE results for eccentrically loaded members; (a) e= H/10, (b) e=H/5, (c) e=H/2, and (d) e=H

Table 4
Comparisons between FE, AISI, and AISI-Re results for eccentrically loaded lipped channels

No.	$e = H/10$		$e = H/5$		$e = H/2$		$e = H$	
	$P_{AISI\text{-}Re}/P_{FE}$	P_{AISI}/P_{FE}	$P_{AISI\text{-}Re}/P_{FE}$	P_{AISI}/P_{FE}	$P_{AISI\text{-}Re}/P_{FE}$	P_{AISI}/P_{FE}	$P_{AISI\text{-}Re}/P_{FE}$	P_{AISI}/P_{FE}
1	0.83	0.73	0.82	0.72	0.83	0.72	0.84	0.72
2	0.84	0.73	0.83	0.72	0.84	0.72	0.85	0.72
3	0.86	0.73	0.85	0.72	0.85	0.72	0.86	0.72
4	0.86	0.74	0.84	0.72	0.84	0.71	0.85	0.72
5	0.85	0.74	0.84	0.73	0.83	0.72	0.84	0.72
6	0.84	0.74	0.83	0.73	0.82	0.72	0.83	0.72
7	0.82	0.73	0.83	0.74	0.81	0.72	0.82	0.72
8	0.81	0.73	0.82	0.74	0.80	0.72	0.81	0.73
9	0.80	0.74	0.80	0.74	0.80	0.73	0.80	0.73
10	0.80	0.74	0.79	0.73	0.80	0.74	0.80	0.74
11	0.79	0.74	0.78	0.74	0.80	0.75	0.80	0.75
12	0.79	0.75	0.78	0.74	0.80	0.76	0.79	0.75
13	0.78	0.75	0.77	0.74	0.79	0.76	0.79	0.76
14	0.78	0.76	0.77	0.75	0.78	0.76	0.79	0.77
15	0.78	0.76	0.77	0.75	0.78	0.76	0.79	0.78
16	0.78	0.77	0.77	0.76	0.77	0.77	0.80	0.79
17	0.78	0.78	0.77	0.76	0.77	0.76	0.80	0.79
18	0.78	0.78	0.77	0.76	0.77	0.76	0.79	0.79
19	0.79	0.78	0.77	0.76	0.77	0.76	0.79	0.79
20	0.79	0.78	0.77	0.76	0.77	0.76	0.79	0.79
Mean	**0.81**	**0.75**	**0.80**	**0.74**	**0.80**	**0.74**	**0.81**	**0.75**
COV	**0.04**	**0.02**	**0.04**	**0.02**	**0.03**	**0.03**	**0.03**	**0.04**

To prove the AISI-Re method's reliability, finite element (FE) results from F. Öztürk et al. [37] are compared with calculated nominal strength according to the aforementioned five design methods. Different major axis eccentric loads are applied to the CFS-lipped-channel beam columns, as described in [37]. Subsequently, the nominal strength (β) parameter is computed as follows:

$$\beta = \sqrt{\left(\frac{M_1}{M_{1y}}\right)^2 + \left(\frac{M_2}{M_{2y}}\right)^2 + \left(\frac{P}{P_y}\right)^2} \tag{16}$$

where $P, M_1,$ and M_2 are the applied axial compression and biaxial bending moments, and $P_y, M_{1y},$ and M_{2y} are the squash load and biaxial yield moments, respectively. The effective performance of AISI-Re is assessed in Fig. 9, with results that agree with the finite element (FE) results in [37]. This further confirms the accuracy and reliability of the AISI-Re method, which prior investigations have supported.

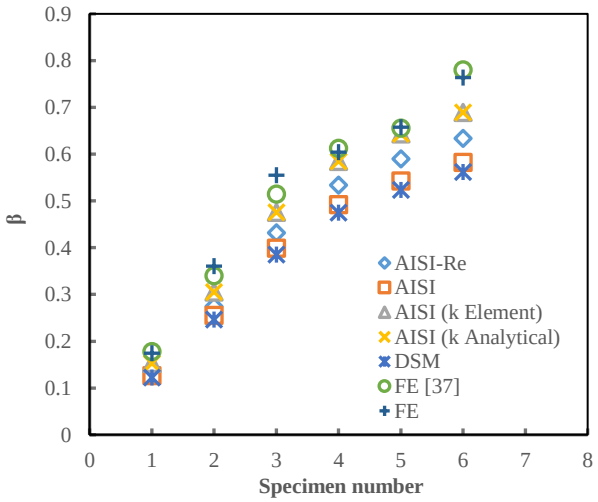

Fig. 9 Comparisons between nominal strength parameters ($\boldsymbol{\beta}$) for lipped channel sections obtained from different design methods and FE results

5.2. Reliability analysis

The proposed method is further evaluated against the FE data in a more quantifiable manner by calculating the reliability index (β_o). The reliability is determined concerning the corresponding resistance factor as follows [15]

$$\phi = C_\phi (M_m F_m P_m) e^{-\beta_o \sqrt{v_m^2 + v_F^2 + C_p V_P^2 + V_Q^2}} \tag{17}$$

where ϕ is the resistance factor, C_ϕ is the calibration factor (=1.52) as implemented in [38], M_m and F_m are the mean value of the material factor (=1.05 and 1.0), respectively for combined axial load and bending, P_m is the mean value of FE-to-predicted ratios, β_o is target reliability index which is taken equal to 2.5 for structural members, V_m and V_F are the coefficient of variation of the material and fabrication factor (= 0.1 and 0.05), respectively, C_p is the correction factor that taken to be 1.0 for reliability analysis, V_P is the coefficient of variation of FE-to-predicted ratios as calculated in Table 5 and V_Q is coefficient of variance for the load effect (= 0.21 for LRFD); see[15].

Results of the reliability analysis are summarized in Table 5, wherein the mean values of FE-to-predicted ratios and the corresponding COV values determine the reliability index for two sets of resistance factors $\phi(= 0.85)$ and $(= 0.9)$. Furthermore, a target reliability index of 2.5 is used to compute the resistance factors. The table reveals that the proposed AISI-Re gives more accurate results than the AISI design method, which is significantly conservative for the studied cross sections. The derived reliability indices of the linear interaction equation in AISI [15] are 3.24 ($\phi = 0.85$) and 3.00 ($\phi = 0.9$) for the AISI-Re design method, which are significantly higher than the desired reliability indices of 2.5. The results indicate that the current specification for predicting the nominal strength [15] needs to be improved by evaluating the plate buckling coefficient (k), as demonstrated in the AISI-Re, to achieve closer results to the validated FE results.

Table 5
Reliability analysis for AISI-Re and current AISI design method

Eccentricity	No.	AISI-Re($\beta_{FE}/\beta n$)					EWM AISI($\beta_{FE}/\beta n$)				
		P_m	V_p	$\beta_o(\varphi=0.85)$	$\beta_o(\varphi=0.9)$	$\varphi(\beta o=2.5)$	P_m	V_p	$\beta_o(\varphi=0.85)$	$\beta_o(\varphi=0.9)$	$\varphi(\beta o=2.5)$
$e=0$	20	1.12	0.010	3.12	2.88	0.986	1.21	0.05	3.38	3.14	1.05
$e=H/10$	20	1.17	0.020	3.30	3.06	1.028	1.26	0.04	3.57	3.33	1.10
$e=H/5$	20	1.17	0.020	3.30	3.06	1.028	1.26	0.04	3.57	3.33	1.10
$e=H/2$	20	1.15	0.010	3.23	2.99	1.012	1.24	0.04	3.50	3.27	1.08
$e=H$	20	1.13	0.010	3.16	2.92	0.994	1.22	0.05	3.41	3.17	1.06
All	100	1.15	0.017	3.24	3.00	1.01	1.24	0.04	3.50	3.27	1.08

6. Conclusions and summary

This paper aims to establish a practical design for cold-formed steel-lipped-channel cross-sections, offering a framework to enhance the existing codified effective width method (EWM). An AISI-Re design approach is proposed, incorporating an assessed and validated k-value for local plate buckling. A parametric study is undertaken to evaluate the impact of the local plate buckling coefficient on the design of cold-formed steel (CFS) lipped channel cross-sections with varying (H/B) ratios, whether utilizing the codified EWM or the recent direct strength method (DSM). Additionally, results obtained from a validated finite element (FE) model are presented as benchmark solutions for the nominal strength of the analyzed members. Based on the generated results, the proposed AISI-Re design, which takes into account the interaction between adjacent sub-elements through the local plate buckling coefficient (i.e., k-value), demonstrates enhanced accuracy and reliability. Conclusions drawn from the results presented in this paper are as follows:

- The local buckling coefficient (k) significantly influences elastic and inelastic buckling strength calculation for cold-formed steel (CFS) lipped-channel cross-sections.
- Considering the restraining effect between sectional sub-elements is essential for adjacent sub-elements, as it expresses boundary conditions that substantially impact the plate buckling coefficient.
- The direct strength method (DSM) is regarded as a more reliable approach than the effective width method (EWM) in pure compression loading conditions, and its effectiveness can be further enhanced by incorporating a more realistic and accurate k-factor.
- AISI-Re can be seen as an improved method aligning with existing AISI standards. It provides realistic buckling strengths and closely aligns with experimental test results.
- The refined k-factors demonstrate a notable effect within the range of $1 \leq (H/B) \leq 2$ compared to the existing AISI values.

Acknowledgments

The second author is grateful for financial support from the competitive research projects - research unit - Mansoura University for the project ‘‘Solar Energy Storage System Using a Medium of Sustainable Geopolymer Concrete’’ (MU-Eng-22-15).

References

[1] A. D. Martins, D. Camotim, and P. B. Dinis, “Local-distortional interaction in cold-formed steel beams: Behaviour, strength and DSM design,” *Thin-Walled Struct.*, vol. 119, no. August, pp. 879–901, 2017, doi: 10.1016/j.tws.2017.06.011.

[2] M. T. Chen, B. Young, A. D. Martins, D. Camotim, and P. B. Dinis, “Experimental investigation on cold-formed steel stiffened lipped channel columns undergoing local-distortional interaction,” *Thin-Walled Struct.*, vol. 150, no. February, 2020, doi: 10.1016/j.tws.2020.106682.

[3] D. Cava, D. Camotim, P. B. Dinis, and A. Madeo, “Numerical investigation and direct strength design of cold-formed steel lipped channel columns experiencing local-distortional-global interaction,” *Thin-Walled Struct.*, vol. 105, pp. 231–247, 2016, doi: 10.1016/j.tws.2016.03.025.

[4] J. Becque and K. J. R. Rasmussen, “Experimental investigation of local-overall interaction buckling of stainless steel lipped channel columns,” *J. Constr. Steel Res.*, vol. 65, no. 8–9, pp. 1677–1684, 2009, doi: 10.1016/j.jcsr.2009.04.025.

[5] P. B. Dinis, D. Camotim, B. Young, and E. M. Batista, “CFS lipped channel columns affected by L-D-G interaction. Part II: Numerical simulations and design considerations,” *Comput. Struct.*, vol. 207, pp. 200–218, 2018, doi: 10.1016/j.compstruc.2017.03.017.

[6] B. Young, P. B. Dinis, and D. Camotim, “CFS lipped channel columns affected by L-D-G interaction. Part I: Experimental investigation,” *Comput. Struct.*, vol. 207, pp. 219–232, 2018, doi: 10.1016/j.compstruc.2017.03.016.

[7] G. Winter, “Strength of thin steel compression flanges,” *Trans. Am. Soc. Civ. Eng.*, vol. 112, no. 1, pp. 527–554, 1947.

[8] A. Moldovan, “Compression tests on cold-formed steel columns with monosymmetrical section,” *Thin-Walled Struct.*, vol. 20, no. 1–4, pp. 241–252, 1994, doi: 10.1016/0263-8231(94)90068-X.

[9] B. Young, N. Silvestre, and D. Camotim, “Cold-Formed Steel Lipped Channel Columns Influenced by Local-Distortional Interaction: Strength and DSM Design,” *J. Struct. Eng.*, vol. 139, no. 6, pp. 1059–1074, 2013, doi: 10.1061/(asce)st.1943-541x.0000694.

[10] M. Dundu, “Buckling of short cold-formed lipped channels in compression,” *J. South African Inst. Civ. Eng.*, vol. 56, no. 2, pp. 46–53, 2014.

[11] B. W. Schafer, “CUFSM 3.12, elastic buckling analysis of thin-walled members by finite strip analysis.” 2006.

[12] T. L. G. CHEUNG YK, “Finite Strip Method [M].” Boca Raton: CRC Press, 1998.

[13] “Abaqus/CAE User’s Manual, version 6.14-2, USA, 2014.” “Dassault Syst{\`e}mes Simulia Corp.”

[14] *Standards Australia/Standards New Zealand. Cold-formed steel structures, AS/NZS 4600;1996.*

[15] American Iron and Steel Institute, “North American Specification Steel Structural Members,” *North Am. Specif. Steel Struct. Members*, p. 78, 2016.

[16] D. Dubina, R. Landolfo, and V. Ungureanu, “Design of cold-formed steel structures.: Eurocode 3: design of steel structures. Part 1-3, Design of cold-formed steel structures,” 2012.

[17] ECP-205 (LRFD), “Egyptian Code of Practice for Steel Construction.” 2008.

[18] G. H. Bryan, “On the Stability of a Plane Plate under Thrusts in its own Plane, with Applications to the ‘Buckling’ of the Sides of a Ship,” *Proc. London Math. Soc.*, vol. 1, no. 1, pp. 54–67, 1890.

[19] L. Schuman and G. Back, *Strength of rectangular flat plates under edge compression*, no. 356. NACA, 1930.

[20] T. Von Kármán, “Strength of thin plates in compression,” *Trans. ASME*, vol. 54, p. 53, 1932.

[21] B. W. Schafer, “The direct strength method of cold-formed steel member design,” *J. Constr. steel Res.*, vol. 64, no. 7–8, pp. 766–778, 2008.

[22] C. Yu and W. Yan, “Effective Width Method for determining distortional buckling strength of cold-formed steel flexural C and Z sections,” *Thin-Walled Struct.*, vol. 49, no. 2, pp. 233–238, 2011, doi: 10.1016/j.tws.2010.11.006.

[23] G. P. Mulligan and T. Pekoz, “Local buckling interaction in cold-formed columns,” *J. Struct. Eng.*, vol. 113, no. 3, pp. 604–620, 1987.

[24] M. D. Ahdab, A. W. Fischer, C. Ding, B. Glauz, and B. W. Schafer, “Local buckling expressions for lipped channels,” *Struct. Stab. Res. Counc. Conf. 2022, Held conjunction with NASCC Steel Conf.*, pp. 1–17, 2022.

[25] S. Torabian, B. Zheng, and B. W. Schafer, “Experimental response of cold-formed steel lipped channel beam-columns,” *Thin-Walled Struct.*, vol. 89, pp. 152–168, 2015, doi: 10.1016/j.tws.2014.12.003.

[26] K. Roy *et al.*, “Cold-Formed Steel Lipped Channel Section Columns Undergoing Local-Overall Buckling Interaction,” *Int. J. Steel Struct.*, vol. 21, no. 2, pp. 408–429, 2021, doi: 10.1007/s13296-020-00447-w.

[27] A. H. A. Abdelrahman, S. Liu, Y. P. Liu, and S. L. Chan, “Simulation of Thin-Walled Members with Arbitrary-Shaped Cross-Sections for Static and Dynamic Analyses,” *Int. J. Struct. Stab. Dyn.*, vol. 20, no. 12, pp. 1–22, 2020, doi: 10.1142/S021945542050128X.

[28] B. W. Schafer, Z. Li, and C. D. Moen, “Computational modeling of cold-formed steel,” *Thin-Walled Struct.*, vol. 48, no. 10–11, pp. 752–762, 2010, doi: 10.1016/j.tws.2010.04.008.

[29] N. Abdel-Rahman and K. S. Sivakumaran, “Material properties models for analysis of cold-formed steel members,” *J. Struct. Eng.*, vol. 123, no. 9, pp. 1135–1143, 1997.

[30] E. Ellobody and B. Young, “Structural performance of cold-formed high strength stainless steel columns,” vol. 61, pp. 1631–1649, 2005, doi: 10.1016/j.jcsr.2005.05.001.

[31] L. Gardner and X. Yun, “Description of stress-strain curves for cold-formed steels,” *Constr. Build. Mater.*, vol. 189, pp. 527–538, 2018, doi: 10.1016/j.conbuildmat.2018.08.195.

[32] B. Schafer and T. Peköz, “Geometric imperfections and residual stresses for use in the analytical modeling of cold-formed steel members,” *Int. Spec. Conf. Cold-Formed Steel Struct. Recent Res. Dev. Cold-Formed Steel Des. Constr.*, pp. 649–664, 1996.

[33] R. G. Dawson and A. C. Walker, “Post-buckling of geometrically imperfect plates,” *J. Struct. Div.*, vol. 98, no. 1, pp. 75–94, 1972.

[34] Z. Li and B. W. Schafer, “Application of the finite strip method in cold-formed steel member design,” *J. Constr. Steel Res.*, vol. 66, no. 8–9, pp. 971–980, 2010.

[35] M. R. Bambach, “Design of uniformly compressed edge-stiffened flanges and sections that contain them,” *Thin-Walled Struct.*, vol. 47, no. 3, pp. 277–294, 2009, doi: 10.1016/j.tws.2008.07.011.

[36] B. W. Schafer and T. Pekoz, “Direct strength prediction of cold-formed steel members using numerical elastic buckling solutions,” 1998.

[37] F. Öztürk, S. M. Mojtabaei, M. Şentürk, S. Pul, and I. Hajirasouliha, “Buckling behaviour of cold-formed steel sigma and lipped channel beam–column members,” *Thin-Walled Struct.*, vol. 173, no. August 2021, p. 108963, 2022, doi: 10.1016/j.tws.2022.108963.

[38] V. Z. Meimand and B. W. Schafer, “Impact of load combinations on structural reliability determined from testing cold-formed steel components,” *Struct. Saf.*, vol. 48, pp. 25–32, 2014, doi: 10.1016/j.strusafe.2013.10.006.